Optical and Quantum Electronics (2021) 53:544
https://doi.org/10.1007/s11082-021-03203-4

Comparison of optical, electrical, and surface characteristics of InGaN thin films at non-flow and small nitrogen flow cases

Asim Mantarcı[1]

Received: 10 February 2021 / Accepted: 18 August 2021 / Published online: 29 August 2021

Abstract

InGaN films in the non-flow and a small flow of nitrogen cases were fabricated by the RFMS (Radio Frequency Magnetron Sputter) method to compare crucial physical characteristics of its material. From the XRD analysis, application of small nitrogen flow in the InGaN thin film growth has been observed to result in changes in the crystal size, texture coefficient, and crystal structure parameters of the film. AFM results showed both films obtained have tightly packed granular, and almost homogeneous, and Nano-structural properties, but they are different in roughness, as increased by applying small nitrogen flow. Optical conductance peaks of the material in non-flow and small flow case were 1.3957×10^{10} and $1.1496 \times 10^{10}(\mathrm{S/m})$, showed a decrement in optical conductance by small nitrogen flow. In the same manner, electrical conductance peaks of the material in non-flow and small flow case were 5.2512×10^{12} and $5.2236 \times 10^{12}(\mathrm{S})$, showed a decrement in electrical conductance by small nitrogen flow. In addition, the electrical conductivity of the InGaN material has been obtained at higher than the optical conductivity value of the InGaN material in both cases. Also, it was noticed that direct allowed optical band gap energy non-flow and small flow cases were 2.65 and 2.69 eV, displayed increased by applied small nitrogen flow. Essentially, many noteworthy physical properties such as crystalline size, texture coefficient, optical/electrical conductivity, the surface roughness of the films have been compared and studied for the non-flow and a small flow of nitrogen cases. Therefore; a better understanding of the structural/crystal and electrical characteristics of the InGaN film by applying/optimizing different growth conditions will be able to pave the way for InGaN device studies.

Keywords Non-flow · InGaN · Texture coefficient · Electrical conductivity · Nano-structure

✉ Asim Mantarcı
a.mantarci@alparslan.edu.tr; asimmantarci@gmail.com

[1] Physics Department, Muş Alparslan University, Güzeltepe/Muş, Turkey

1 Introduction

InGaN (Indium Gallium Nitride) material, which is included in 3 nitride groups, has been used in device production (micro LEDs, solar water splitting, ultrasensitive strain sensor, etc.) that require high technology and has emitted from the ultraviolet to the green region (Dalapati et al. 2020; Smith et al. 2020; Alizadeh et al. 2020; Hu et al. 2020; Iyer et al. 2020; Chen et al. 2020b; Pasayat et al. 2020; Mantarcı 2021).Theoretically speaking, $In_xGa_{1-x}N$ has a capacity to absorb all photons at region energies covering the entire spectrum from 0.7 eV to 3.4 eV, proved from (Moses et al. 2011). Moreover, the material has high mobility (Yarar 2008) and high absorption coefficient (Schenk et al. 2000) properties, which makes it a potential candidate for manufacturing multi-joint solar cells (approx. > 50% efficiency). Materials used in space applications are required to be resistant to high radiation, and the InGaN material has been proven in this research (Zhang et al. 2013) that its high radiation resistance can be used in space applications. Nowadays, many important InGaN-based devices such as field emitters (Chen et al. 2020a), multicolor display (Evropeitsev et al. 2020), and intermediate band solar cell (Cheriton et al. 2020) are produced. Studies (Yang et al. 2017) in the literature have shown us that the electrical, optical and structural parameters of the InGaN material limit the efficiency of the material for many key parameters such as electron mobility (Gökden et al. 2010) and photon absorption (Liu et al. 2017). Furthermore, when the material is used in an optoelectronic device, the mentioned properties will affect the efficiency of the device. For these reasons, investigating the changes in the structural, electrical and optical properties of the InGaN for different conditions will shed light on the studies to be carried out. In this research, the changes in the electrical, optical and structural properties of the films produced in non-flow and small nitrogen flow cases were compared. The main subject of this work is to understand and compare the effects of different conditions designed while producing the film on the key properties of the film: electrical conductivity, optical conductivity, optical band gap energy, crystal-structure parameters. The innovative aspect of this study is; a better understanding of the structural/crystal and electrical characteristics of the InGaN film by applying or optimizing different growth conditions will be able to pave the way for InGaN device studies.

2 Material and methods

2.1 The growth of the material

InGaN thin films in the non-flow and a small flow of nitrogen case were coated onto GaN/n-Si (100) substrate, which was previously published by our research team (Mantarcı,Kundakçi 2019). Films with the best properties among the films produced before were used as substrates. The target used in the study (the InGaN target (99.99% (4n) purity, 3.18 × 50 mm)) was obtained from the ACI Alloys Comp. In the research center called DAYTAM, the films were produced by the sputtering system (VAKSIS, 3 M- RF sputter) in the Clean room. In preparation for the film growth stage, the substrates were cleaned by HF: DI (1:1) processing, the detailed procedure of which is given in the reference (Smith et al. 1996). The coating process was as follows respectively. First, the cleaned substrates were placed in the holder in the system. The system was put into the initial vacuum. When the initial vacuum is reached, the working gas (argon gas) was given to the system. The

system was powered up and the plasma was ignited. The surface was pre-sputtered for about 10 min before the growth was initiated. More details about the growth process can be found in the reference in another study (Mantarcı and Kundakçi 2020).The following are the parameters applied in the coating. The initial pressure is $\sim 5 \times 10^{-3}$mTorr, argon as a working gas (50 sccm), target to substrate angle ~ 31.0°, target to substrate distance 12.3 cm, substrate temperature 500 ℃, substrate rotation 3 rpm, the sputtering power is 100 W. During growth, the coating parameters of the films were kept constant except that the small nitrogen flow (1 sccm) was applied to one of the films. To do this, the change of coating parameters was monitored instantly by an automatic control panel.

2.2 Characterization of the material

Surface topography properties of materials were determined using Hitachi 5100 N–AFM from the 5 μm × 5 μm area using the tapping mode in which the tip was hit on the surface. The absorption properties of the materials of non-flow and small flow cases were investigated using a Shimadzu UV-3600 Plus spectrophotometer. This system has Pbs and InGaAs detectors and an R-928 model photomultiplier. The main monochromator is of high-performance holographic grating type in aberration-corrected Czerny-Turner mounting. XRD technique (D-8, PANalytical Empyrean) was used to understand the crystal-structure properties of films. Grazing incidence mode (GI-XRD) was preferred while taking measurements. Here are our XRD operate parameters; generator voltage = 45 kV, omega = 0.5, psi = 0, Phi = 0, z = 9.329, time per step = 2.64 s, tube current = 40 mA, the anode material = Cu, K-Alpha1 wavelength = 1.5405980 A°, K-Alpha2 wavelength = 1.5444260 A°. The thickness measurements of the obtained films were made with the KlaTencor Stylus Profiler P7. The resolution in the vertical axis was 1 A° and the repeatability of step thickness measurement in the Z-axis was 0.5 nm. The thickness of the films obtained was measured to be 93 nm within error ± 2 nm.

3 Results and discussion

3.1 Structure-crystal properties

X-ray diffraction patterns of the material in non-flow and small flow cases are shown in Fig. 1(a, b). According to the PDF card no: 98-018-1363 (supplementary file), films with a polycrystalline structure ((002) XRD phase and (011) XRD phase) were obtained. The discussion about the reason for the formation of the (011) phase can be noteworthy and is explained following. The published study (Thompson and Carel 1995) said that distribution of crystallographic orientations in polycrystalline film can evolve via many kinetic processes. Orientation evolution has occurred before, during, and after coalescence of islands to form a continuous film, during thickening of a film, and during post-deposition annealing. Final orientation of our film have depended on which texture-selection mechanisms and driving forces dominate, and has been different for different films, substrates, and deposition condition (Thompson and Carel 1995). It is possible to calculate crystallite sizes using Scherrer law (Patterson 1939) and it is given as follows;

$$D = k \cdot \lambda / (\mathrm{FWHM}) \cdot \mathrm{Cos}\theta \tag{1}$$

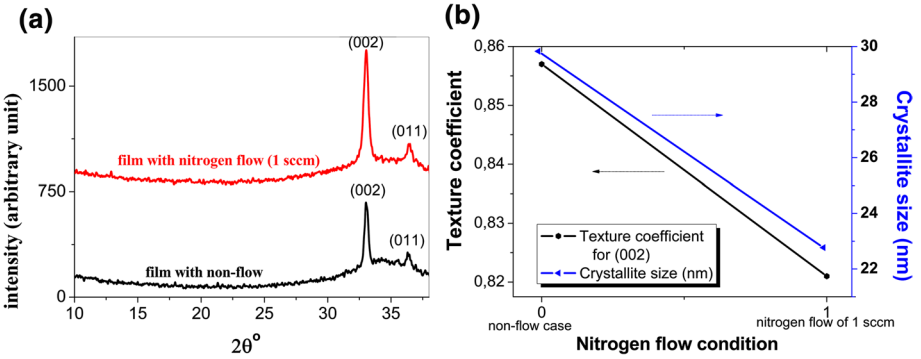

Fig. 1 **a** X-ray diffraction patterns of the material in non-flow and small flow cases (**b**) The change of texture coefficient and crystallite size depending on non-flow and small flow cases

Θ is the diffraction angle of Bragg, k = 0.94 is constant, the FWHM is full-width of half maximum intensity, λ is X-ray wavelength (see in experimental section), D is the crystallite size. From Scherrer law, crystallite sizes of the films for (002) phase were obtained to be 29.83 (±0.6) and 22.77 (±0.3) nm at non-flow and small nitrogen flow case as a decreased trend. Using Bragg law (Bragg, 1913), inter-planar spacing (d), lattice parameters (a, c) of thin films can be calculated as seen formula 2;

$$d_{\mathrm{hkl}} = \frac{\lambda}{\left(2\sin\theta_{\mathrm{hkl}}\right)}; \quad \frac{1}{d_{\mathrm{hkl}}} = \sqrt{\frac{4}{3}\left(\frac{h^2 + h.k + k^2}{a^2}\right) + \frac{l^2}{c^2}} \tag{2}$$

where hkl shows miller indices. Thanks to Bragg's law, inter-planar spacing (d) was calculated to be 2.7120 and 2.7080 Å, and lattice parameters (a, c) were calculated to be 3.3214, 5.4240 and 3.3165, 5.4160 Å, as can be seen in Table 1, they are close to the theoretical values. Indium ratio can be estimated by famous Vegard's Law (Vegard 1921) using the following relation (3);

$$x = \frac{(c_o(\mathrm{InGaN}) - c_o(\mathrm{GaN}))}{(c_o(\mathrm{InN}) - c_o(\mathrm{GaN}))} \tag{3}$$

C_o(InGaN) is the lattice parameter (c) of InGaN, c_o(GaN) is the lattice parameter (c) of GaN and C_o(InN) is the lattice parameter (c) of InN. The above formula allows estimating the indium ration (x) in the $In_xGa_{1-x}N$ structure. As a comparison, the non-flow film has an $In_{0.4846}Ga_{0.5154}$ N film structure; the small nitrogen flow film has an $In_{0.4690}Ga_{0.5310}$ N film structure. This result may be mainly due to a decrement in $c_{o\ (InGaN)}$ value. In addition, the elemental composition of the film in a small nitrogen flow case was obtained from the XPS survey spectrum and a very near value was obtained and consistent with our calculated value (see in supplemental Table S1). A statistical entity of crystalline orientations in the polycrystalline is defined as the crystallographic texture of the material. To put it another way; it expresses deviations from the statistical randomness of preferred orientations. With the Harris texture theorem stated in the past study (Harris 1952), the texture coefficient ($C_{(t)}$) of our films can be determined. On the one hand; texture coefficients for (002) orientation, which is a preferred orientation, were 0.857 and 0.821 at non-flow and small nitrogen flow cases, respectively, showing a decreasing trend. A decrease in preferred orientation is associated with a decreased number of crystallites along that plane. On the other hand,

Table 1 Comparison of crystal-structure properties of films under the condition of non-flow and small Nitrogen flow

Nitrogen flow condition	FWHM (°) (002)	Crystallite size (Scherrer) (nm) (002)	Lattice constants ^{E} (002) (Å)	Lattice constants ^{T} (002) (Å)	d-value ^{E} (Å)	d-value ^{T} (Å)	$2\theta^{E}$ (°)	$2\theta^{T}$ (°)
			a	a				
			c	c				
Non-flow	0.29 ± 0.09	29.83 ± 0.6	3.3214 ± 0.01	3.3300	2.7120 ± 0.01	2.6995	33.00	33.15
			5.4240 ± 0.01	5.3990				
Nitrogen flow of 1 sccm	0.38 ± 0.07	22.77 ± 0.3	3.3165 ± 0.01	3.3300	2.7080 ± 0.01	2.6995	33.05	33.15
			5.4160 ± 0.01	5.3990				

texture coefficients for (011) orientation were 0.142 and 0.178 at non-flow and small nitrogen flow cases, respectively, showing an increasing trend. An increase in preferred orientation is associated with an increased number of crystallites along that plane. In a polycrystalline film, both surface and interface energy minimization support the development of texture via preferred growth of crystallite by specific orientation (Thompson 1990). The final texture depends on growth conditions (including total pressure, power supplied to the target, substrate, and its temperature) and growth techniques. Also, it should be good to discuss why the crystal size decreases when applied a small nitrogen flow. The crystallite size of thin-film depends on nucleation and growth kinetics during processing (Dammers and Radelaar 1992). It may be different for different processing. Many growth parameters affect the crystallite size of the thin film (for example, substrate temperature, working pressure, etc.). Due to the above study, it also very risks saying that the exact reason for decrease crystallite size. However, one of the reasons could be that applying a small nitrogen flow leads to crystal having increased surface energy; therefore decrease in crystallite size (Thompson 1990). Briefly, the application of small nitrogen flow in the InGaN thin film growth has been observed to result in changes in the crystal size, texture coefficient, and crystal structure parameters of the film.

3.2 Surface -topographic properties

RMS (Root Mean Square) roughness of films at non-flow and small flow case were 38.02, 45.67 nm, respectively, as increased with applying small nitrogen flow. This increase in surface roughness can be attributed to the decrease hill widths on GaN surfaces due to increased nitrogen flow, explained the end of this section in detail. Figure 2 gives AFM surface features of thin-film for (a) non-flow case (b) small flow case. As can be seen in Fig. 2a, b, both films obtained have tightly packed, granular, and almost homogeneous and Nano-structural properties. Film at small flow case has more white areas than in non-flow case may be due to white rust and oxide on the surface (Bilgili et al. 2018). Other surface topographic properties of films (surface maximum valley depth, surface absolute slope, etc.) are given in Table S2 as supplemental information. The discussion about the change of roughness with the introduction of a small nitrogen flow can be useful. The surface of our substrate show distinct island growth, see in the published work (Mantarcı and Kundakçi 2019). The morphology of GaN island affects the growth of the InGaN film and the roughness of the film. The study (Bilgili et al. 2018) said that the surface roughness of the InGaN film is closely related to hill widths

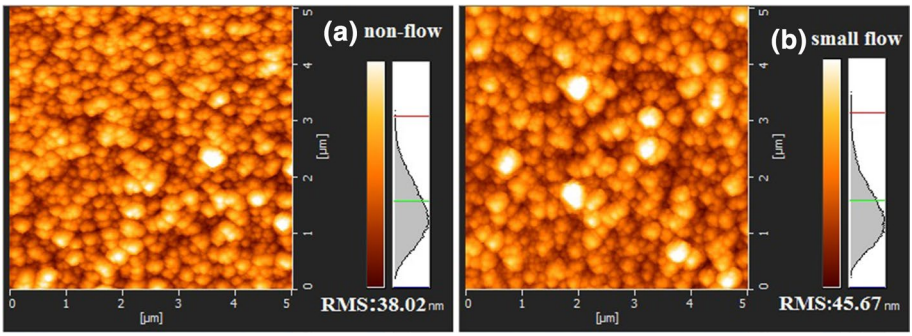

Fig. 2 AFM surface features of thin-film for (**a**) non-flow case (**b**) small flow case

on GaN surfaces. As hill width decrease surface roughness increase. With the introduction of a small nitrogen flow, the roughness of the InGaN film increased. This increase may be attributed to decrease hill widths on GaN surfaces by applying small nitrogen flow.

3.3 Optical band gap energy and absorbance properties

Figure 3a, b gives the Absorbance and Tauc plot of thin-film for non-flow case and small flow case. Using Tauc theory from $\alpha^2E^2 - E$ plot (intersect value in the y-axis at zero), the optical band gap energies of films can be determined. By drawing Fit Linear in the Origin Pro 8 program, direct allowed optical band gap energy in the non-flow and small flow cases were 2.65 and 2.69 eV, displayed increased by applied small nitrogen flow. This increase in optical band gap energy may be due to the difference in indium ratio in films. In the past published article (Özen et al. 2016), the direct -allowed optical band gap energy of the InGaN was found to be 2.75 eV and this value is bigger than the value we found. The refractive index values of films at non-flow and small flow cases can be calculated with some theorems (Moss 1985), (Ravindra et al. 2007), (Hervé and Vandamme 1994), and Kumar and Singh (2010) using the optical band gap energy. The refractive indices of thin films decrease when the small nitrogen flow is given. This decrease may be attributed to the decrease in optical absorption when the small nitrogen flow is given. This explanation is supported by the study (Xue et al. 2008). The obtained refractive index values are given in the supplementary document (Table S3).

3.4 Optical/electrical conductivity properties

Studying the electrical (Qashou et al. 2019) and optical conductivity (Roknuzzaman et al. 2017) behavior of materials plays a key role in optoelectronic device studies; can be described with the following formulas;

$$\sigma_{(\text{electr.})} = (2\lambda) \cdot \left(\sigma_{(\text{opt.})}\right) \cdot (\alpha)^{-1} \tag{4}$$

$$\sigma_{(\text{opt.})} = (\alpha \text{nc}) \cdot (4\pi)^{-1} \tag{5}$$

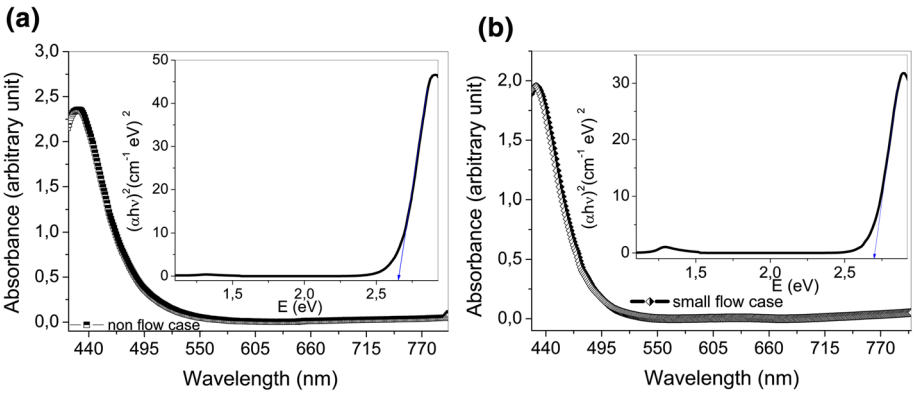

Fig. 3 Absorbance and Tauc plot of thin-film for (**a**) non-flow case (**b**) small flow case

where n, the refractive index for Moss model. The change of optical conductance and electrical conductance parameter depending on non-flow and small flow cases are shown in Fig. 4a, b. In the energy range of 2.1 to 3.9 eV, optical conductance peaks of the material in non-flow and small flow case were 1.3957×10^{10} and 1.1496×10^{10}(Siemens/m), showed a decrement in optical conductance by small nitrogen flow. In a work (Berrah et al. 2009) published in the literature, the optical conductivity of the material was obtained a little higher than our value. In the energy range of $\sim 2.4 - 3.5$ eV, electrical conductance peaks of the material in non-flow and small flow case were 5.2512×10^{12} and 5.2236×10^{12}(Siemens), showed a decrement in electrical conductance by small nitrogen flow. In a past published article (Hu et al. 2010), the electrical conductivity of the material was found to be higher than our value. The electrical conductivity of the InGaN material has been obtained at higher than the optical conductivity value of the InGaN material in both non-flow and small flow cases. In summary, applying small nitrogen flow to the film causes a reducing change in electrical and optical conductivity values.

4 Conclusions

InGaN films in the non-flow and a small flow of nitrogen cases were fabricated by the RFMS method to compare noteworthy physical characteristics of its material. XRD proved that films with a polycrystalline structure ((002) XRD phase and (011) XRD phase) were obtained. Crystallite sizes of the films for the (002) phase were obtained to be 29.83 (±0.6) and 22.77 nm(±0.3) at non-flow and small nitrogen flow case as a decreased trend. As a comparison, the non-flow film has an $In_{0.4846}Ga_{0.5154}$ N film structure; the small nitrogen flow film has an $In_{0.4690}Ga_{0.5310}$ N film structure. This result may be mainly due to a decrement in $c_{o\ (InGaN)}$ value. On the one hand; texture coefficients for (002) orientation, which is a preferred orientation, were 0.857 and 0.821 at non-flow and small nitrogen flow cases, respectively, showing a decreasing trend. A decrease in preferred orientation is associated with a decreased number of crystallites along that plane. On the other hand, texture coefficients for (011) orientation were 0.142 and 0.178 at non-flow and small nitrogen flow cases, respectively, showing an increasing trend. An increase in preferred orientation is associated with an increased number of crystallites along that plane. RMS (Root Mean Square) roughness of films at non-flow and small flow case were 38.02, 45.67 nm,

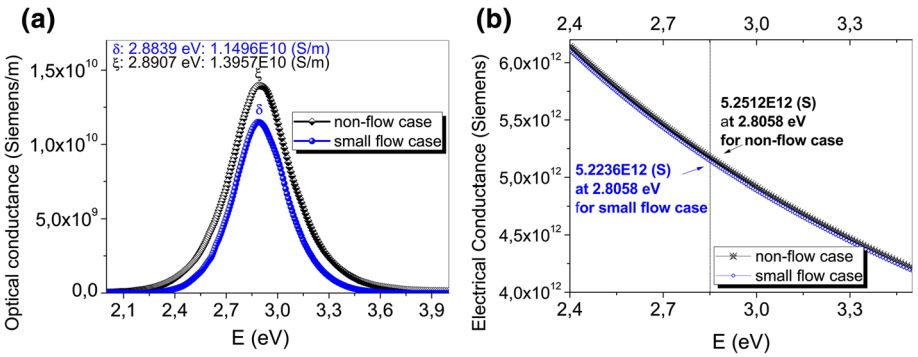

Fig. 4 The change of (**a**) optical conductance (**b**) electrical conductance parameter depending on non-flow and small flow cases

respectively, as increased with applying small nitrogen flow. This increase in surface roughness can be attributed to the decrease hill widths on GaN surfaces due to increased nitrogen flow. Film at small flow case has more white areas than in non-flow case may be due to white rust and oxide on the surface. Direct allowed optical band gap energy in the non-flow and small flow cases were 2.65 and 2.69 eV, showed an increase by applied small nitrogen flow. This increase in optical band gap energy may be due to the difference in indium ratio in films. Optical conductance peaks of the material in non-flow and small flow case were 1.3957×10^{10} and 1.1496×10^{10}(S/m), showed a decrement in optical conductance by small nitrogen flow. In the same manner, electrical conductance peaks of the material in non-flow and small flow case were 5.2512×10^{12} and 5.2236×10^{12}(S), showed a decrement in electrical conductance by small nitrogen flow. Shortly, application of small nitrogen flow in the InGaN thin film growth has been observed to result in changes in the crystal size, texture coefficient, and optical/electrical conductivity and surface roughness of the film, which will be able to shed light on InGaN-based studies.

Supplementary Information The online version contains supplementary material available at https://doi.org/10.1007/s11082-021-03203-4.

Acknowledgements This project was funded by the Muş Alparslan University Research Council (MUS-BAP) (with Project No: BAP-20-VMYO-4901-01)

Author contributions The author (Asim Mantarcı) did all processes: conception or design of the work, data collection, data analysis, and interpretation, drafting the article, critical revision of the article, final approval of the version to be published.

Data availability Supplementary file is available for this study.

Declarations

Conflict of interest There is no conflict of interest in this study.

References

Alizadeh, M., Tong, G.B., Qadir, K.W., Mehmood, M.S., Rasuli, R.: Cu2O/InGaN heterojunction thin films with enhanced photoelectrochemical activity for solar water splitting. Renew. Energy **156**, 602–609 (2020). https://doi.org/10.1016/j.renene.2020.04.107

Berrah, S., Boukortt, A., Abid, H.: Optical properties of the cubic alloy (In, Ga)N. Phys. e: Low-Dimens. Syst. Nanostruct. **41**(4), 701–704 (2009). https://doi.org/10.1016/j.physe.2008.11.009

Bilgili, A.K., Akpınar, Ö., Öztürk, M.K., Başköse, C., Özçelik, S., Özbay, E.: Investigation of structural, optical and morphological properties of InGaN/GaN structure. Appl. Phys. A **125**(1), 36 (2018). https://doi.org/10.1007/s00339-018-2338-2

Bragg, W.H., Bragg, W.L.: The reflection of X-rays by crystals. Proc. r. Soc. Lond. Ser. a, Contain. Pap. Math. Phys. Character **88**(605), 428–438 (1913). https://doi.org/10.1098/rspa.1913.0040

Chen, F., Ji, X., Lau, S.P.: Recent progress in group III-nitride nanostructures: from materials to applications. Mater. Sci. Eng. r. Rep. **142**, 100578 (2020a). https://doi.org/10.1016/j.mser.2020.100578

Chen, L., Zhang, K., Dong, J., Wang, B., He, L., Wang, Q., He, M., Wang, X.: The piezotronic effect in InGaN/GaN quantum-well based microwire for ultrasensitive strain sensor. Nano Energy **72**, 104660 (2020b). https://doi.org/10.1016/j.nanoen.2020.104660

Cheriton, R., Sadaf, S.M., Robichaud, L., Krich, J.J., Mi, Z., Hinzer, K.: Two-photon photocurrent in InGaN/GaN nanowire intermediate band solar cells. Commun. Mater. **1**(1), 63 (2020). https://doi.org/10.1038/s43246-020-00054-6

Dalapati, P., Manik, N.B., Basu, A.N.: Temperature dependence of current–voltage and carrier lifetime characteristics in InGaN blue light-emitting diode. Opt. Quant. Electron. **52**(2), 54 (2020). https://doi.org/10.1007/s11082-019-2182-4

Dammers, A.J., Radelaar, S.: A grain growth model for evolution of polycrystalline surfaces. Mater. Sci. Forum **94–96**, 345–350 (1992)

Evropeitsev, E.A., Kazanov, D.R., Robin, Y., Smirnov, A.N., Eliseyev, I.A., Davydov, V.Y., Toropov, A.A., Nitta, S., Shubina, T.V., Amano, H.: State-of-the-art and prospects for intense red radiation from core–shell InGaN/GaN nanorods. Sci. Rep. **10**(1), 19048 (2020). https://doi.org/10.1038/s41598-020-76042-0

Gökden, S., Tülek, R., Teke, A., Leach, J.H., Fan, Q., Xie, J., Özgür, Ü., Morkoç, H., Lisesivdin, S.B., Özbay, E.: Mobility limiting scattering mechanisms in nitride-based two-dimensional heterostructures with the InGaN channel. Semicond. Sci. Technol. **25**(4), 045024 (2010). https://doi.org/10.1088/0268-1242/25/4/045024

Harris, G.B.: X. Quantitative measurement of preferred orientation in rolled uranium bars. Lond. Edinb. Dublin Philos. Mag. J. Sci. **43**(336), 113–123 (1952). https://doi.org/10.1080/14786440108520972

Hervé, P., Vandamme, L.K.J.: General relation between refractive index and energy gap in semiconductors. Infrared Phys. Technol. **35**(4), 609–615 (1994). https://doi.org/10.1016/1350-4495(94)90026-4

Hu, H., Tang, B., Wan, H., Sun, H., Zhou, S., Dai, J., Chen, C., Liu, S., Guo, L.J.: Boosted ultraviolet electroluminescence of InGaN/AlGaN quantum structures grown on high-index contrast patterned sapphire with silica array. Nano Energy **69**, 104427 (2020). https://doi.org/10.1016/j.nanoen.2019.104427

Hu, Y.-J., Huang, Y.-W., Fang, C.-H., Wang, J.-C., Chen, Y.-F., Nee, T.-E.: Anomalous disorder-related phenomena in InGaN/GaN multiple quantum well heterosystems. J. Lumin. **130**(6), 1000–1004 (2010). https://doi.org/10.1016/j.jlumin.2010.01.014

Iyer, P.P., DeCrescent, R.A., Mohtashami, Y., Lheureux, G., Butakov, N.A., Alhassan, A., Weisbuch, C., Nakamura, S., DenBaars, S.P., Schuller, J.A.: Unidirectional luminescence from InGaN/GaN quantum-well metasurfaces. Nat. Photonics **14**(9), 543–548 (2020). https://doi.org/10.1038/s41566-020-0641-x

Kumar, V., Singh, J.: Model for calculating the refractive index of different materials. Indian J. Pure Appl. Phys. **48**, 571–574 (2010)

Liu, W.H., Qu, Y., Ban, S.L.: Electron mobility limited by optical phonons in wurtzite InGaN/GaN core-shell nanowires. J. Appl. Phys. **122**(11), 115104 (2017). https://doi.org/10.1063/1.5003261

Mantarcı, A., Kundakçi, M.: Physical properties of RF magnetron sputtered GaN/n-Si thin film: impacts of RF power. Opt. Quant. Electron. **51**(3), 81 (2019). https://doi.org/10.1007/s11082-019-1795-y

Mantarcı, A., Kundakçi, M.: Production of GaN/n–Si thin films using RF magnetron sputtering and determination of some physical properties: argon flow impacts. J. Aust. Ceram. Soc. **56**(3), 905–914 (2020). https://doi.org/10.1007/s41779-019-00420-9

Mantarcı, A.: Investigation of changes in structural properties of polycrystalline $In_{0.6628}Ga_{0.3372}N$ thin film. Appl. Phys. A **127**, 469 (2021). https://doi.org/10.1007/s00339-021-04631-5

Moses, P.G., Miao, M., Yan, Q., Walle, C.G.V.D.: Hybrid functional investigations of band gaps and band alignments for AlN, GaN, InN, and InGaN. J. Chem. Phys. **134**(8), 8470 (2011). https://doi.org/10.1063/1.3548872

Moss, T.S.: Relations between the refractive index and energy gap of semiconductors. Physica Status Solidi (b) **131**(2), 415–427 (1985). https://doi.org/10.1002/pssb.2221310202

Özen, S., Şenay, V., Pat, S., Korkmaz, Ş: The influence of voltage applied between the electrodes on optical and morphological properties of the InGaN thin films grown by thermionic vacuum arc. Scanning **38**(1), 14–20 (2016). https://doi.org/10.1002/sca.21237

Pasayat, S.S., Gupta, C., Wong, M.S., Wang, Y., Nakamura, S., Denbaars, S.P., Keller, S., Mishra, U.K.: Growth of strain-relaxed InGaN on micrometer-sized patterned compliant GaN pseudo-substrates. Appl. Phys. Lett. **116**(11), 111101 (2020). https://doi.org/10.1063/5.0001480

Patterson, A.L.: The Scherrer formula for X-ray particle size determination. Phys. Rev. **56**(10), 978–982 (1939). https://doi.org/10.1103/PhysRev.56.978

Qashou, S.I., El-Zaidia, E.F.M., Darwish, A.A.A., Hanafy, T.A.: Methylsilicon phthalocyanine hydroxide doped PVA films for optoelectronic applications: FTIR spectroscopy, electrical conductivity, linear and nonlinear optical studies. Phys. B **571**, 93–100 (2019). https://doi.org/10.1016/j.physb.2019.06.063

Ravindra, N.M., Ganapathy, P., Choi, J.: Energy gap–refractive index relations in semiconductors – an overview. Infrared Phys. Technol. **50**(1), 21–29 (2007). https://doi.org/10.1016/j.infrared.2006.04.001

Roknuzzaman, M., Ostrikov, K., Wang, H., Du, A., Tesfamichael, T.: Towards lead-free perovskite photovoltaics and optoelectronics by ab-initio simulations. Sci. Rep. **7**(1), 14025 (2017). https://doi.org/10.1038/s41598-017-13172-y

Schenk, H.P.D., Leroux, M., Mierry, P.D.: Luminescence and absorption in InGaN epitaxial layers and the van Roosbroeck-Shockley relation. J. Appl. Phys. **88**(3), 1525–1534 (2000). https://doi.org/10.1063/1.373850

Smith, J.M., Ley, R., Wong, M.S., Baek, Y.H., Kang, J.H., Kim, C.H., Gordon, M.J., Nakamura, S., Speck, J.S., DenBaars, S.P.: Comparison of size-dependent characteristics of blue and green InGaN micro-LEDs down to 1 μm in diameter. Appl. Phys. Lett. **116**(7), 071102 (2020). https://doi.org/10.1063/1.5144819

Smith, L.L., King, S.W., Nemanich, R.J., Davis, R.F.: Cleaning of GaN surfaces. J. Electron. Mater. **25**(5), 805–810 (1996). https://doi.org/10.1007/BF02666640

Thompson, C.V.: Grain growth in thin films. Annu. Rev. Mater. Sci. **20**(1), 245–268 (1990). https://doi.org/10.1146/annurev.ms.20.080190.001333

Thompson, C.V., Carel, R.: Texture development in polycrystalline thin films. Mater. Sci. Eng. B **32**(3), 211–219 (1995). https://doi.org/10.1016/0921-5107(95)03011-5

Vegard, L.: Die Konstitution der Mischkristalle und die Raumfüllung der Atome. Z. Phys. **5**(1), 17–26 (1921). https://doi.org/10.1007/BF01349680

Xue, S.W., Zu, X.T., Zhou, W.L., Deng, H.X., Xiang, X., Zhang, L., Deng, H.: Effects of post-thermal annealing on the optical constants of ZnO thin film. J. Alloy. Compd. **448**(1), 21–26 (2008). https://doi.org/10.1016/j.jallcom.2006.10.076

Yang, H., Ma, Z., Jiang, Y., Wu, H., Zuo, P., Zhao, B., Jia, H., Chen, H.: The enhanced photo absorption and carrier transportation of InGaN/GaN quantum wells for photodiode detector applications. Sci. Rep. **7**(1), 43357 (2017). https://doi.org/10.1038/srep43357

Yarar, Z.: Electron mobility in modulation doped AlGaN/GaN and InGaN/GaN quantum wells: a comparative study. Solid State Commun. **147**(3), 98–102 (2008). https://doi.org/10.1016/j.ssc.2008.05.006

Zhang, L.M., Li, C.X., Zhao, J.T., Yang, K.J., Zhang, G.F., Wang, T.S., Zhang, C.H.: Study of radiation damage in InGaN and AlGaN films induced by 8.9 MeV Bi33+ ions. Nucl. Instrum. Methods Phys. Res. Sect. B Beam Interact. Mater. Atoms **305**, 1–4 (2013). https://doi.org/10.1016/j.nimb.2013.04.042